Hindawi
Complexity
Volume 2019, Article ID 5968984, 14 pages
https://doi.org/10.1155/2019/5968984

Research Article

Coordinate Control of Power/Current for Grid-Connected Inverter Based on PCI Controller under Unbalanced Grid Conditions

Chencong Zhao,[1] **Jun Liu**,[1] **Zhouhua Xie**,[2] **and Feihang Zhou**[1]

[1]*College of Automation, Xi'an University of Technology, No. 5 Jinhua South Road, Xi'an, China*
[2]*Thermal Power Research Institute CO LTD, No. 136 Xingqing Road, Xi'an, China*

Correspondence should be addressed to Jun Liu; liujun0310@sina.com

Received 15 March 2019; Revised 23 April 2019; Accepted 27 May 2019; Published 11 July 2019

Academic Editor: Thach Ngoc Dinh

The oscillations on output power and distortion of the inverter currents will occur in the case of unbalanced grid voltage faults. Constant output power and good current quality cannot be achieved simultaneously. Aiming at these problems, a coordinate control strategy for suppressing power fluctuations and current harmonics is proposed by analyzing instantaneous power control and current balance control. The proposed control is achieved by adjusting the weight coefficient of current reference values to change the current harmonic contents based on proportional complex integral (PCI) controller and proportional multiple complex integral (PMCI) controller. The control strategy with a simple control structure neither needs to detect harmonic components of the inverter currents, nor needs to separate the positive and negative components of voltage and current, which is easy to be realized. The feasibility and effectiveness of the proposed control are verified by the comparison and analysis of simulation.

1. Introduction

With the problem of global climate increasingly serious and nonrenewable resources being largely consumed, the development of renewable energy has attracted much attention. Among the many renewable energy sources, the installed capacity of wind energy is increasing year by year because of abundant resources, good industrial foundation, and low environmental pollution. The grid-connected inverter, as the grid-connected interface between wind turbine and large-scale energy storage system, plays an important role in the grid-connected control of wind power system [1–4]. The operation of the grid-connected inverter is susceptible to the unbalanced grid voltage. The causes of unbalanced voltage are various: the interference of high-power single-phase load, the unbalanced distribution of single-phase load in grid and randomness of the single-phase load, etc. [5, 6]. The oscillations on output power and distortion of the inverter currents will occur under unbalanced grid faults [7, 8]. If there is a serious harmonic distortion in the three-phase currents, it may not meet the IEEE Std.1547 standard that the current THD is more than 5%. Therefore, it is important to study the control strategy for grid-connected inverter under unbalanced grid voltage, which is of great significance for stable and efficient operation of the system.

Many control strategies for grid-connected inverter under unbalanced grid voltage have been proposed [5, 6, 9–20]. The traditional control strategy is the dual current vector control in the positive and negative sequence reference frames, and this method is applied in [9–11], by controlling the positive and negative components of voltage and current to eliminate oscillations on the active power. But the realization of this control objective is based on the injection of negative sequence currents, which will inevitably result in harmonics distortion in three-phase inverter currents, and the oscillations on reactive power have not been eliminated. In order to obtain constant output active and reactive powers, a control scheme is proposed which utilizes the resonance compensation method without considering the distortion of inverter currents [12–14]. An interesting control method which utilizes the positive and negative sequence components is proposed in [15] for generating

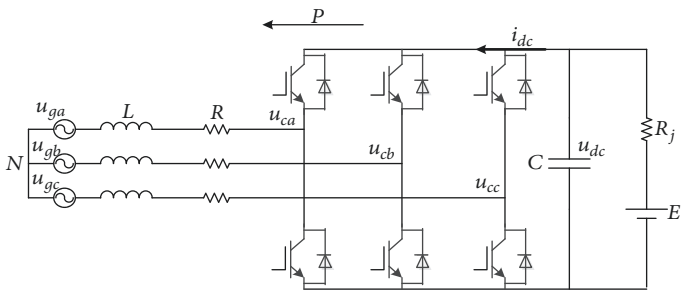

Figure 1: Circuit topology of the grid-connected inverter.

current reference values to reduce the imbalance of grid voltage. But this method mainly aims at current quality; the problem of power oscillations has not been solved under unbalanced grid voltage. For the three control targets, which are aimed at suppressing active power oscillations, reactive power oscillations, and negative current components, a coordinate control of power and current is proposed in [16, 17] where the current references are unified by introducing the coefficients, and the coordinate control is realized by adjusting the coefficients. However, the method requires positive and negative sequence separation and complex reference frame transformation. In addition, the method includes a large number of PI controllers, and parameters tuning is not easy to implement. In order to reduce the complexity of control, the current references of coordinate control can be obtained in $\alpha\beta$ stationary reference frame [5, 6, 18, 19]. A scheme is proposed in [20], which analyzes the power fluctuations and current harmonics magnitude quantitatively. Notch filter is used in the control, and the coordinate control of output power and current quality is realized by using the idea of weighting. The control strategy can reduce the harmonic contents in inverter currents. However, due to the introduction of negative sequence components in the calculation of current references, the balanced three-phase currents cannot be obtained.

In this paper, the instantaneous power control and current balance control are introduced when the grid voltage is unbalanced. The essential relationships between the two control strategies are discussed and the causes of current harmonics are analyzed. On these bases, a novel control strategy is proposed, which uses PCI and PMCI controllers to control inverter currents. Weight coefficient is introduced in current references to change the harmonic contents in inverter currents, and the coordinate control of power fluctuations suppression and current balance is realized. The proposed control does not need complicated reference frame transformation, positive/negative sequence extraction calculation, and notch filter, and it is convenient to realize in the stationary reference frame.

This paper is organized as follows: Section 2 formulates the model of grid-connected inverter. Section 3 analyzes the conventional control schemes and the relationships between the two conventional control schemes. Section 4 analyzes the proposed coordinate control strategy under unbalanced grid voltage. Section 5 shows the simulation results under different cases when the grid voltage is unbalanced, which validates the proposed scheme. Section 6 concludes this paper.

2. Model of Grid-Connected Inverter

Figure 1 shows the topology of grid-connected inverter. u_{ga}, u_{gb}, and u_{gc} are the grid voltages, u_{ca}, u_{cb}, and u_{cc} are the output voltages of the grid-connected inverter, L and R are the inductance and resistance, respectively, and u_{dc} is the dc-link voltage.

The control structure of grid-connected inverter is shown in Figure 2. The power will be transmitted to the grid through the effective control of voltage and current.

3. Conventional Control Strategies

3.1. Voltage Expressions under Unbalanced Grid Voltage. The three-phase unbalanced grid voltages can be expressed as

$$\begin{bmatrix} u_{ga} \\ u_{gb} \\ u_{gc} \end{bmatrix} = \begin{bmatrix} U^+ \sin\left(\omega t + \theta^+\right) + U^- \sin\left(\omega t + \theta^-\right) \\ U^+ \sin\left(\omega t - \frac{2\pi}{3} + \theta^+\right) + U^- \sin\left(\omega t + \frac{2\pi}{3} + \theta^-\right) \\ U^+ \sin\left(\omega t + \frac{2\pi}{3} + \theta^+\right) + U^- \sin\left(\omega t - \frac{2\pi}{3} + \theta^-\right) \end{bmatrix} \tag{1}$$

where U^+ and U^- are the amplitudes of positive and negative components of voltage; θ^+ and θ^- are initial phase angles of the positive and negative components, respectively; ω is the grid frequency.

Unbalanced grid voltage can be transformed into $\alpha\beta$ stationary reference frame as follows:

$$\begin{bmatrix} u_{g\alpha} \\ u_{g\beta} \end{bmatrix} = \frac{2}{3} \begin{bmatrix} 1 & -\frac{1}{2} & -\frac{1}{2} \\ 0 & \frac{\sqrt{3}}{2} & -\frac{\sqrt{3}}{2} \end{bmatrix} \begin{bmatrix} u_{ga} \\ u_{gb} \\ u_{gc} \end{bmatrix} = \begin{bmatrix} u_{g\alpha}^+ + u_{g\alpha}^- \\ u_{g\beta}^+ + u_{g\beta}^- \end{bmatrix} \tag{2}$$

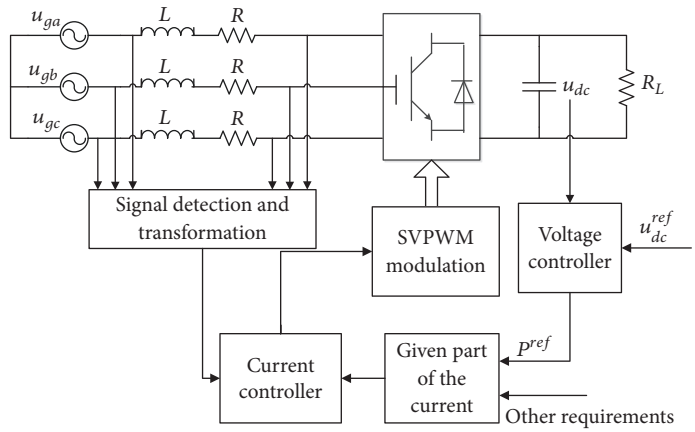

Figure 2: Control structure of grid-connected inverter.

where

$$\begin{bmatrix} u_{g\alpha}^{+} \\ u_{g\beta}^{+} \\ u_{g\alpha}^{-} \\ u_{g\beta}^{-} \end{bmatrix} = \begin{bmatrix} U^{+}\sin\left(\omega t + \theta^{+}\right) \\ -U^{+}\cos\left(\omega t + \theta^{+}\right) \\ U^{-}\sin\left(\omega t + \theta^{-}\right) \\ U^{-}\cos\left(\omega t + \theta^{-}\right) \end{bmatrix} \tag{3}$$

3.2. Instantaneous Power Control Strategy. Based on instantaneous power theory, the active power and reactive power can be expressed as

$$\begin{bmatrix} P \\ Q \end{bmatrix} = \frac{3}{2}\begin{bmatrix} u_{g\alpha} & u_{g\beta} \\ u_{g\beta} & -u_{g\alpha} \end{bmatrix}\begin{bmatrix} i_{\alpha} \\ i_{\beta} \end{bmatrix} \tag{4}$$

where i_{α} and i_{β} are the current components in $\alpha\beta$ stationary frame, respectively.

With the power references P^{*} and Q^{*}, the current reference values can be calculated as follows:

$$\begin{bmatrix} i_{\alpha} \\ i_{\beta} \end{bmatrix} = \frac{2}{3}\begin{bmatrix} u_{g\alpha} & u_{g\beta} \\ u_{g\beta} & -u_{g\alpha} \end{bmatrix}^{-1}\begin{bmatrix} P^{*} \\ Q^{*} \end{bmatrix} \tag{5}$$

From (5), the current references under instantaneous power control can be obtained as follows:

$$\begin{aligned} \begin{bmatrix} i_{\alpha gl}^{*} \\ i_{\beta gl}^{*} \end{bmatrix} &= \begin{bmatrix} i_{\alpha gl(p)} \\ i_{\beta gl(p)} \end{bmatrix} + \begin{bmatrix} i_{\alpha gl(q)} \\ i_{\beta gl(q)} \end{bmatrix} \\ &= \frac{2}{3}\frac{P^{*}}{u_{g\alpha}^{2} + u_{g\beta}^{2}}\begin{bmatrix} u_{g\alpha} \\ u_{g\beta} \end{bmatrix} + \frac{2}{3}\frac{Q^{*}}{u_{g\alpha}^{2} + u_{g\beta}^{2}}\begin{bmatrix} u_{g\beta} \\ -u_{g\alpha} \end{bmatrix} \end{aligned} \tag{6}$$

where $i_{\alpha gl(p)}$ and $i_{\beta gl(p)}$ are the active current components on α-axis and β-axis, respectively; $i_{\alpha gl(q)}$ and $i_{\beta gl(q)}$ are the reactive current components.

Substituting (2) into (6), the denominator in (6) can be expressed as

$$\begin{aligned} u_{g\alpha}^{2} + u_{g\beta}^{2} &= \left(u_{g\alpha}^{+} + u_{g\alpha}^{-}\right)^{2} + \left(u_{g\beta}^{+} + u_{g\beta}^{-}\right)^{2} \\ &= U^{+2} + U^{-2} - 2U^{+}U^{-}\cos\left(2\omega t + \theta^{+} + \theta^{-}\right) \end{aligned} \tag{7}$$

It can be known that $U^{-} \neq 0$ under unbalanced grid voltage, so the existence of $2U^{+}U^{-}\cos(2\omega t + \theta^{+} + \theta^{-})$ term in (7) will result in a large amount of harmonic currents.

Based on the above analysis, it can be seen that the instantaneous power control can maintain a constant output power, but there is severe harmonics distortion in the inverter currents.

3.3. Current Balance Control Strategy. In order to obtain balanced three-phase inverter currents, the negative sequence current components must be eliminated, and the current references under the current balance control strategy can be obtained as follows:

$$\begin{aligned} \begin{bmatrix} i_{\alpha dl}^{*} \\ i_{\beta dl}^{*} \end{bmatrix} &= \begin{bmatrix} i_{\alpha dl(p)} \\ i_{\beta dl(p)} \end{bmatrix} + \begin{bmatrix} i_{\alpha dl(q)} \\ i_{\beta dl(q)} \end{bmatrix} \\ &= \frac{2}{3}\frac{P^{*}}{u_{g\alpha}^{+2} + u_{g\beta}^{+2}}\begin{bmatrix} u_{g\alpha}^{+} \\ u_{g\beta}^{+} \end{bmatrix} + \frac{2}{3}\frac{Q^{*}}{u_{g\alpha}^{+2} + u_{g\beta}^{+2}}\begin{bmatrix} u_{g\beta}^{+} \\ -u_{g\alpha}^{+} \end{bmatrix} \end{aligned} \tag{8}$$

where $i_{\alpha dl(p)}, i_{\beta dl(p)}$ and $i_{\alpha dl(q)}, i_{\beta dl(q)}$ are the active and reactive current components, respectively.

It can be seen that the current references do not contain harmonic terms, and the sinusoidal and balanced inverter currents can be obtained. It should be noted that the negative sequence current components are eliminated, but the negative sequence voltage components still exist in the voltage when the grid voltage is unbalanced. The interaction between the negative sequence voltage components and the positive sequence current components will result in double frequency fluctuations on the output power.

3.4. Analysis of the Two Control Strategies. Based on the above analysis, it is known that instantaneous power control or current balance control cannot achieve constant output power and balanced inverter currents simultaneously.

In order to analyze the relationships between the current references under the two control strategies, suppose that the initial phase angle $\theta^{+} = \theta^{-} = 0$. Firstly, the active current components on α-axis are discussed as an example. The

active current references under the two control strategies are expressed as

$$i_{\alpha gl(p)} = \frac{2}{3}\frac{u_{g\alpha}P^*}{u_{g\alpha}^2 + u_{g\beta}^2} = \frac{2}{3}\frac{\left(U^+ + U^-\right)P^* \sin \omega t}{\left(U^+\right)^2 + \left(U^-\right)^2 - 2U^+U^- \cos\left(2\omega t\right)} \tag{9}$$

$$i_{\alpha dl(p)} = \frac{2}{3}\frac{u_{g\alpha}^+}{u_{g\alpha}^{+2} + u_{g\beta}^{+2}}P^* = \frac{2}{3}\frac{\sin \omega t}{U^+}P^* \tag{10}$$

From (9) and (10), it can be seen that $i_{\alpha gl(p)}$ is a nonsinusoidal periodic signal, and $i_{\alpha dl(p)}$ is a fundamental sinusoidal signal. According to Fourier theory, $i_{\alpha gl(p)}$ can be decomposed into a superposition of fundamental and harmonic signals as follows:

$$i_{\alpha gl(p)} = \frac{a_0}{2} + \sum_{n=1}^{\infty}\left[a_n \cos\left(n\omega t\right) + b_n \sin\left(n\omega t\right)\right] \tag{11}$$

The coefficients a_n and b_n can be expressed as

$$a_n = \frac{2}{T}\int_{-T/2}^{T/2} f\left(t\right)\cos\left(n\omega t\right)dt; \quad n = 0, 1, 2\cdots\infty$$
$$b_n = \frac{2}{T}\int_{-T/2}^{T/2} f\left(t\right)\sin\left(n\omega t\right)dt; \quad n = 1, 2\cdots\infty \tag{12}$$

where $T = 2\pi$. It is clear that $i_{\alpha gl(p)}$ is an odd function, $a_n = 0$ can be obtained according to the nature of odd function, and the fundamental frequency component of $i_{\alpha gl(p)}$ can be expressed as

$$i_{\alpha gl(p)}^f = b_1 \sin \omega t \tag{13}$$

where $b_1 = (2P^*/3\pi)\int_{-\pi}^{\pi}(u_{g\alpha}/(u_{g\alpha}^2 + u_{g\beta}^2))\sin(\omega t)d\omega t = 2P^*/3U^+$.

From (10) and (13), the following equation can be obtained:

$$i_{\alpha gl(p)}^f = \frac{2P^*}{3U^+}\sin \omega t = i_{\alpha dl(p)} \tag{14}$$

For the sake of simplicity, this conclusion is obtained under the assumption of $\theta^+ = \theta^- = 0$, but the same conclusion can be obtained through Fourier decomposition when $\theta^+ = \theta^- \neq 0$. Similarly, the fundamental components of $i_{\alpha gl(q)}$, $i_{\beta gl(p)}$, and $i_{\beta gl(q)}$ can be calculated, and compared with the current references under current balance control, the essential relationships of the current references can be obtained as follows:

$$i_{\beta gl(p)}^f = i_{\beta dl(p)}$$
$$i_{\alpha gl(q)}^f = i_{\alpha dl(q)} \tag{15}$$
$$i_{\beta gl(q)}^f = i_{\beta dl(q)}$$

By combining (14) and (15), the current relationships can be obtained as follows:

$$i_{\alpha gl}^f = i_{\alpha dl}$$
$$i_{\beta gl}^f = i_{\beta dl} \tag{16}$$

From (16), it can be seen that the fundamental components of current references under instantaneous power control are equivalent to the current references under current balance control, and three-phase currents are balanced. This is the essential relationship of current reference values between the two control strategies and it will lay the foundation for the design of control strategy in the next section.

4. Coordinate Control of Power/Current Design of Controller

The current references include the fundamental and harmonic components under instantaneous power control, and the current fundamental components are equivalent to the current reference values under current balance control. The current harmonic components are composed of the low-order harmonics such as third, fifth, and seventh harmonics, etc. [20]. Harmonic contents will affect the degree of power fluctuations suppression and current balance. Therefore, the coordinate control of power and current can be achieved by adjusting the harmonic contents in three-phase currents under instantaneous power control. Based on the analysis, a coordinate control scheme is proposed to control the fundamental and harmonic currents simultaneously. The references of fundamental components $i_{\alpha\beta}^{f*}$ and harmonic components $i_{\alpha\beta}^{h*}$ can be calculated as follows:

$$\begin{bmatrix} i_\alpha^{f*} \\ i_\beta^{f*} \end{bmatrix} = \frac{2}{3}\frac{P^*}{u_{g\alpha}^2 + u_{g\beta}^2}\begin{bmatrix} u_{g\alpha} \\ u_{g\beta} \end{bmatrix} + \frac{2}{3}\frac{Q^*}{u_{g\alpha}^2 + u_{g\beta}^2}\begin{bmatrix} u_{g\beta} \\ -u_{g\alpha} \end{bmatrix} \tag{17}$$

$$\begin{bmatrix} i_\alpha^{h*} \\ i_\beta^{h*} \end{bmatrix} = k\begin{bmatrix} i_\alpha^{f*} \\ i_\beta^{f*} \end{bmatrix} \tag{18}$$

The current references under instantaneous power control are represented in (17), and P^* and Q^* are the output active and reactive power references. The value of k in (18) is the weight coefficient. If $k = 0$, there are no harmonic components in the inverter currents, which means current balance control; it is equivalent to instantaneous power control when $k = 1$. The output active and reactive powers are constant, but the inverter currents contain lots of harmonics ($i_{\alpha\beta}^{h*} = i_{\alpha\beta}^{f*}$); the control effect is between the effect of instantaneous power control and current balance control when $0<k<1$. As the value of k increases from 0 to 1, the harmonic contents in currents will increase gradually, but the output power will tend to be constant.

The control structure of proposed control strategy is shown in Figure 3.

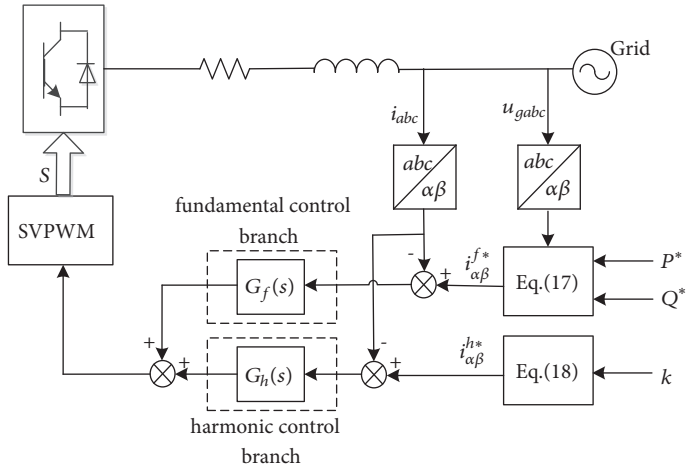

Figure 3: The diagram of system control structure.

4.1. PCI Controller. As mentioned above, the proposed control can be implemented in the stationary reference frame. The fundamental current component in the fundamental control branch and the harmonic current components in the harmonic control branch need to be controlled, respectively. Therefore, the scheme based on the PCI controller is proposed [21].

The transfer function of the PCI controller can be expressed as

$$G_f(s) = K_p + \frac{K_i}{s - j\omega} \tag{19}$$

where K_p and K_i represent proportional and integral coefficients, respectively. Due to the existence of plural in the transfer function, it is not easy to realize. According to the complex function theory, j means that the amplitude is constant and the phase rotates 90° counterclockwise. Based on the orthogonal relationship (i.e., $m_\alpha = j\, m_\beta$) in $\alpha\beta$ reference frame, the complex domain controller can be realized by the structure, as shown in Figure 4.

Figure 5 is the bode diagram of the PCI controller. It can be seen that there is an infinite gain at the fundamental frequency (i.e., 50 Hz) and there are almost no gains in the rest of the frequency bands, so the fundamental component in the inverter currents can be controlled precisely by the PCI controller.

The harmonic components in inverter currents should also be controlled. Based on the PCI controller, PMCI controller is proposed to suppress the harmonic components.

The transfer function of PMCI controller can be expressed as

$$G_h(s) = K_{ph} + \frac{K_{i3}}{s - j3\omega} + \frac{K_{i5}}{s - j5\omega} + \frac{K_{i7}}{s - j7\omega} \tag{20}$$

Figure 6 shows the bode diagram of the PMCI controller. The gains are infinite at the third, fifth, and seventh harmonic frequencies, while the gains are not increased significantly in the other frequency bands. Hence, the controller can be used to suppress the low-order harmonic components in the inverter currents effectively.

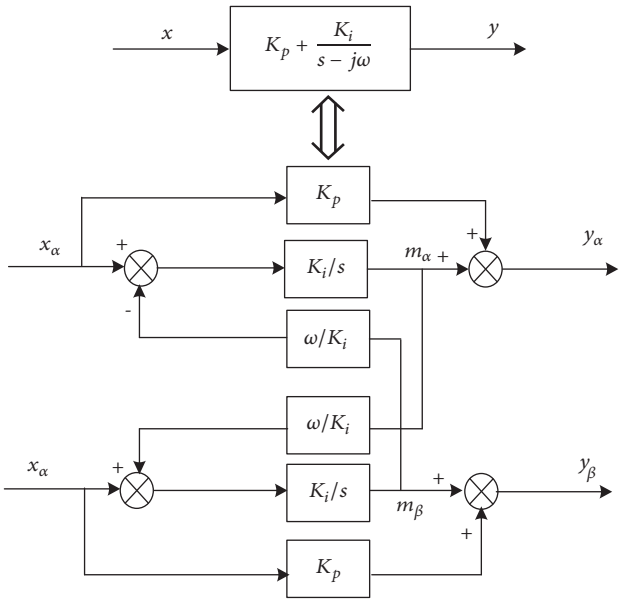

Figure 4: The structure diagram of PCI controller.

4.2. Performance Analysis of Proposed Control. According to the control scheme mentioned above, current inner loop control structure is shown in Figure 7, where, $G_f(s)$ and $G_h(s)$ represent the transfer functions of fundamental and harmonic controllers, respectively. K_{PWM} is the equivalent gain of the PWM converter and it is often taken as $K_{PWM} = U_{dc}/2$. U_g represents the grid voltage.

According to Figure 7, the output current can be obtained as follows:

$$i_{\alpha\beta} = X_f i^{f*}_{\alpha\beta} + X_h i^{h*}_{\alpha\beta} - X_u U_g \tag{21}$$

Table 1: Main parameters of the grid-side system.

Parameters	Value
Unbalanced voltages U_a, U_b, U_c/V (case a)	$217\angle 90^\circ, 311\angle -30^\circ, 311\angle -150^\circ$
Unbalanced voltages U_a, U_b, U_c/V (case b)	$217\angle 85^\circ, 296\angle -28^\circ, 323\angle -150^\circ$
Unbalanced voltages U_a, U_b, U_c/V (case c)	$0\angle 0^\circ, 311\angle -30^\circ, 311\angle -150^\circ$
Grid side inductance, L/H	0.006
Grid side resistance, R/Ω	0.1
DC-link voltage, U_{dc}/V	800
DC-link capacitor, C/F	0.003
Current fundamental control branch, K_p/K_i	0.3/300
Current harmonic control branch, $K_{ph}/K_{i3}/K_{i5}/K_{i7}$	100/20/20/20

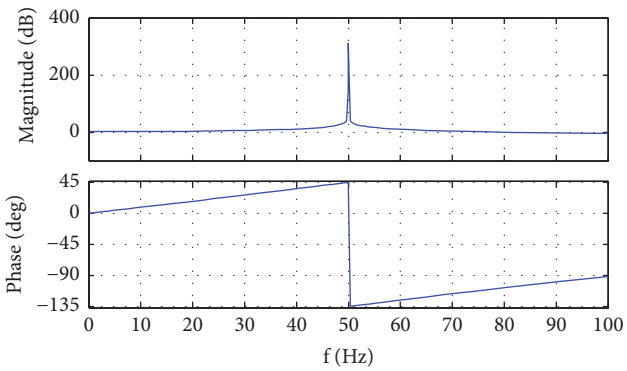

Figure 5: The bode diagram of $G_f(s)$.

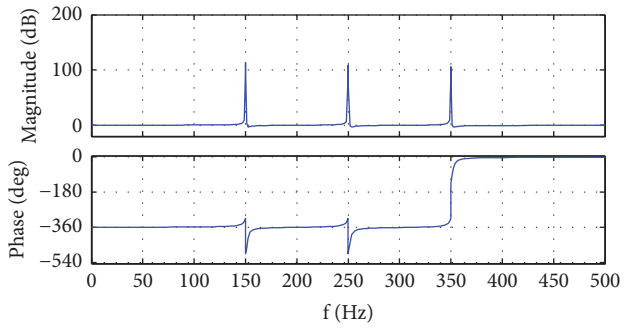

Figure 6: The bode diagram of $G_h(s)$.

where X_f denotes the transfer function between the output current and reference of current fundamental component, X_h denotes the transfer function between the output current and reference of current harmonic components, and X_u denotes the transfer function between the output current and grid voltage, which can be expressed as

$$X_f = \frac{G_f K_{PWM}}{Ls + R + G_h K_{PWM} + G_f K_{PWM}}$$

$$X_h = \frac{G_h K_{PWM}}{Ls + R + G_h K_{PWM} + G_f K_{PWM}}$$

$$X_u = \frac{1}{Ls + R + G_h K_{PWM} + G_f K_{PWM}} \quad (22)$$

Based on the main parameters of the system in Table 1, the bode diagrams of transfer functions between the output current and different input reference signals can be obtained, respectively, as shown in Figures 8–10, and the control performances of proposed control strategy are analyzed.

Figure 8 shows the amplitude-frequency and phase-frequency characteristic curves of closed-loop transfer function $X_f(s)$. It can be seen that the difference of tracking gain and phase at fundamental frequency (i.e., 50 Hz) tend to be 0 dB and 0°, respectively. Therefore, the inverter currents can track the fundamental component of reference signal $i^{f*}_{\alpha\beta}$ with equal amplitude. Similarly, the amplitude gains are attenuated greatly at the third, fifth, and seventh harmonic frequencies, which indicates that the inverter currents have almost no ability to track low-order harmonics of reference signal $i^{f*}_{\alpha\beta}$.

The amplitude-frequency and phase-frequency characteristic curves of closed-loop transfer function $X_h(s)$ are shown in Figure 9. As can be seen from the figure, the gain at the grid fundamental frequency is attenuated greatly. On the contrary, the differences of tracking gains and phases at the third, fifth, and seventh harmonic frequencies are close to 0 dB and 0°, respectively. It indicates that the inverter currents can track the harmonic components of reference signal $i^{h*}_{\alpha\beta}$ accurately. However, the fundamental component of the $i^{h*}_{\alpha\beta}$ can be tracked hardly. Similarly, the amplitude-frequency and phase-frequency characteristic curves of closed-loop transfer function $X_u(s)$ are shown in Figure 10. The grid voltage is equivalent to a disturbance component. From Figure 10, the tracking gains at the fundamental and low-order harmonic frequencies are very small, and the influences on the inverter currents can be neglected.

Based on superposition theorem and the above graphic analysis, it can be seen that the proposed control can control

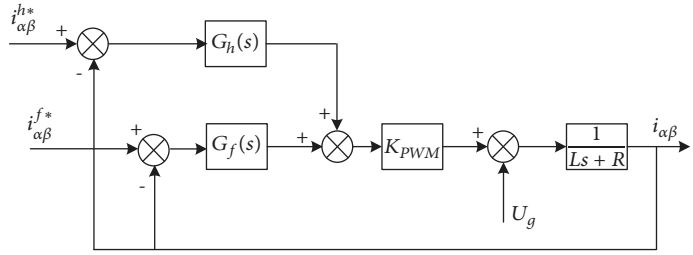

Figure 7: The structure diagram of current inner loop.

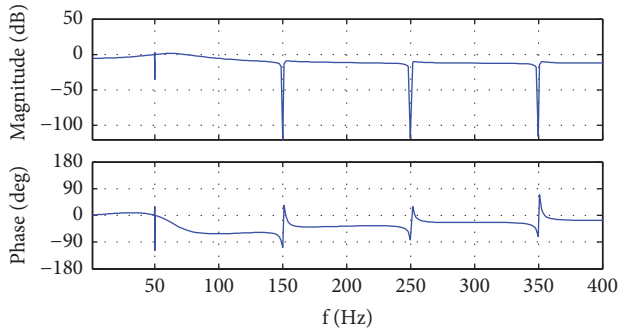

Figure 8: The bode diagram of $X_f(s)$.

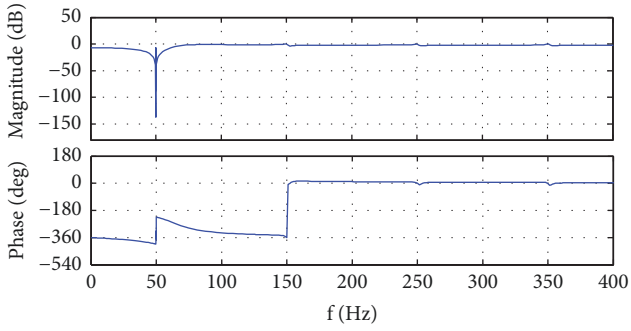

Figure 9: The bode diagram of $X_h(s)$.

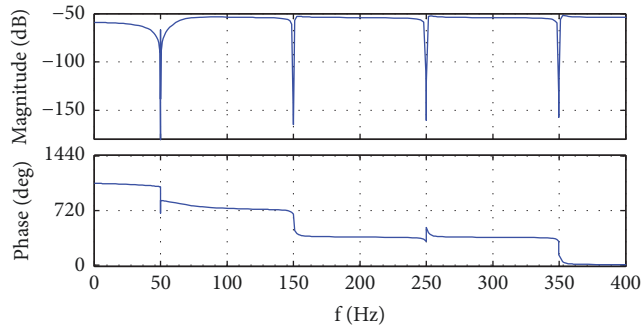

Figure 10: The bode diagram of $X_u(s)$.

three-phase inverter currents effectively. The fundamental component of $i^{f*}_{\alpha\beta}$ affects the fundamental component of inverter currents, and the low-order harmonic components of $i^{h*}_{\alpha\beta}$ affect the low-order harmonic components of inverter currents. Therefore, this control strategy needn't detect the low-order harmonic components of inverter currents by adjusting the weight coefficient in the references of currents to realize the control of harmonic currents, and the coordinate control of power and current is realized.

5. Simulation Results

In this section, simulations are carried out with MATLAB/Simulink environment. Figure 11 shows the grid voltages that change from a balanced condition to an unbalanced condition in three different cases. Figure 11(a) shows the grid voltage that 30% voltage dip in phase A during the period from 0.1 s to 0.5 s. Figure 11(b) shows the three-phase voltages with unbalanced amplitude and phase offset. Figure 11(c) shows the unbalanced grid voltage when phase A is short circuited to the ground.

Figure 12 shows the simulation results by using the instantaneous power control under three different unbalanced voltages. From Figure 12, it can be seen that the output active and reactive powers are constant during the period of 0.1 s~0.5 s. The dc-link voltage is relatively smooth, and there are almost no double-frequency fluctuations on output power, but the three-phase inverter currents are distorted obviously. Taking phase A current as an example, harmonic spectrum analysis is carried out. It can be seen that the total harmonic current distortion (THD) is large in the three cases (i.e., 10.31%, 11.39%, and 23.65%, respectively), which does not meet the THD standard of less than 5% stipulated by the IEEE Std.1547. In the three cases, the proportions of the third harmonic are reached: 10.21%, 11.28%, and 23.04%, respectively. Therefore, if the instantaneous power control strategy is adopted, the output active and reactive powers are constant, but there is a serious distortion in the inverter currents.

Figure 13 shows the simulation results by using current balance control in the three different cases. From Figure 13, it can be seen that there are obvious fluctuations on the output active power, reactive power, and dc-link voltage when the three-phase voltages are unbalanced (0.1 s~0.5 s). However, the three-phase currents are balanced and sinusoidal. From the harmonic analysis of phase A current, it can be seen that the THD is 1.15% in case a, 1.39% in case b, and 2.95% in case c; the third harmonic only accounted for 0.8%, 0.86%, and 2.57%, respectively. The results satisfy the THD standard

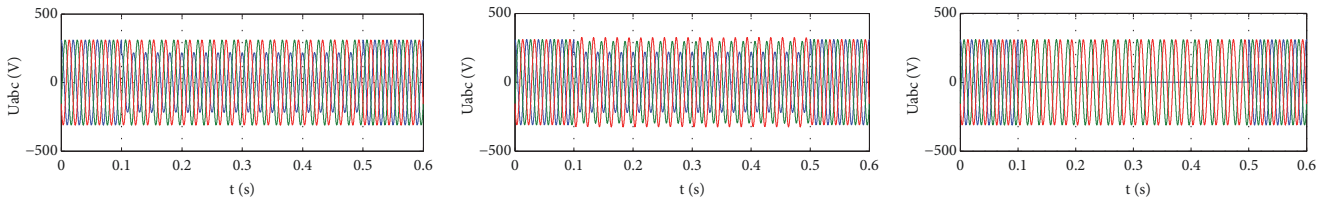

(a) Case a (b) Case b (c) Case c

Figure 11: The unbalanced grid voltages in different cases.

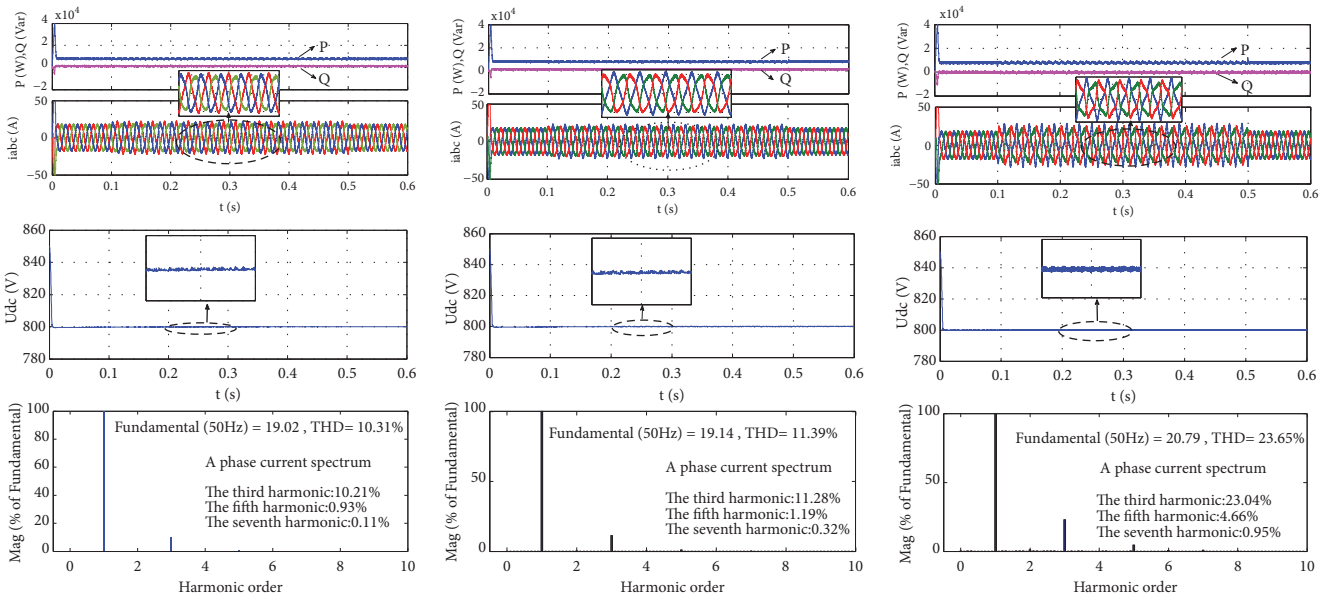

(a) Case a (b) Case b (c) Case c

Figure 12: Simulation results of instantaneous power control strategy in different cases.

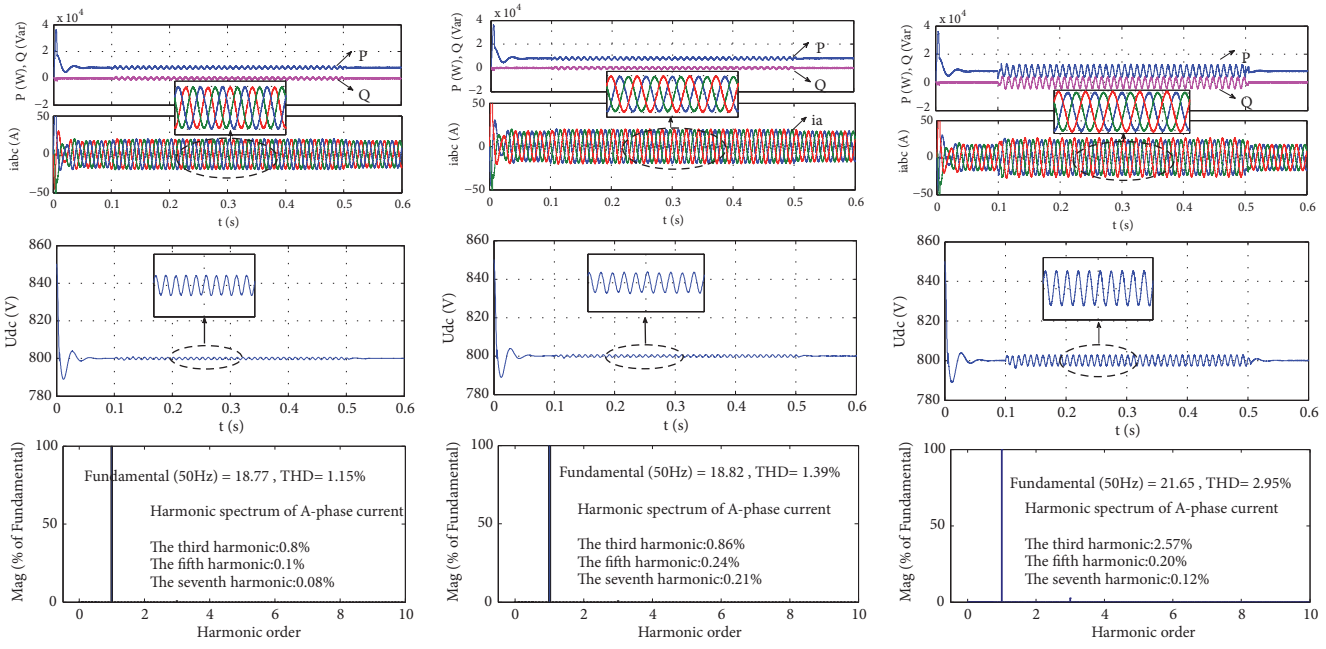

(a) Case a (b) Case b (c) Case c

Figure 13: Simulation results of current balance control strategy in different cases.

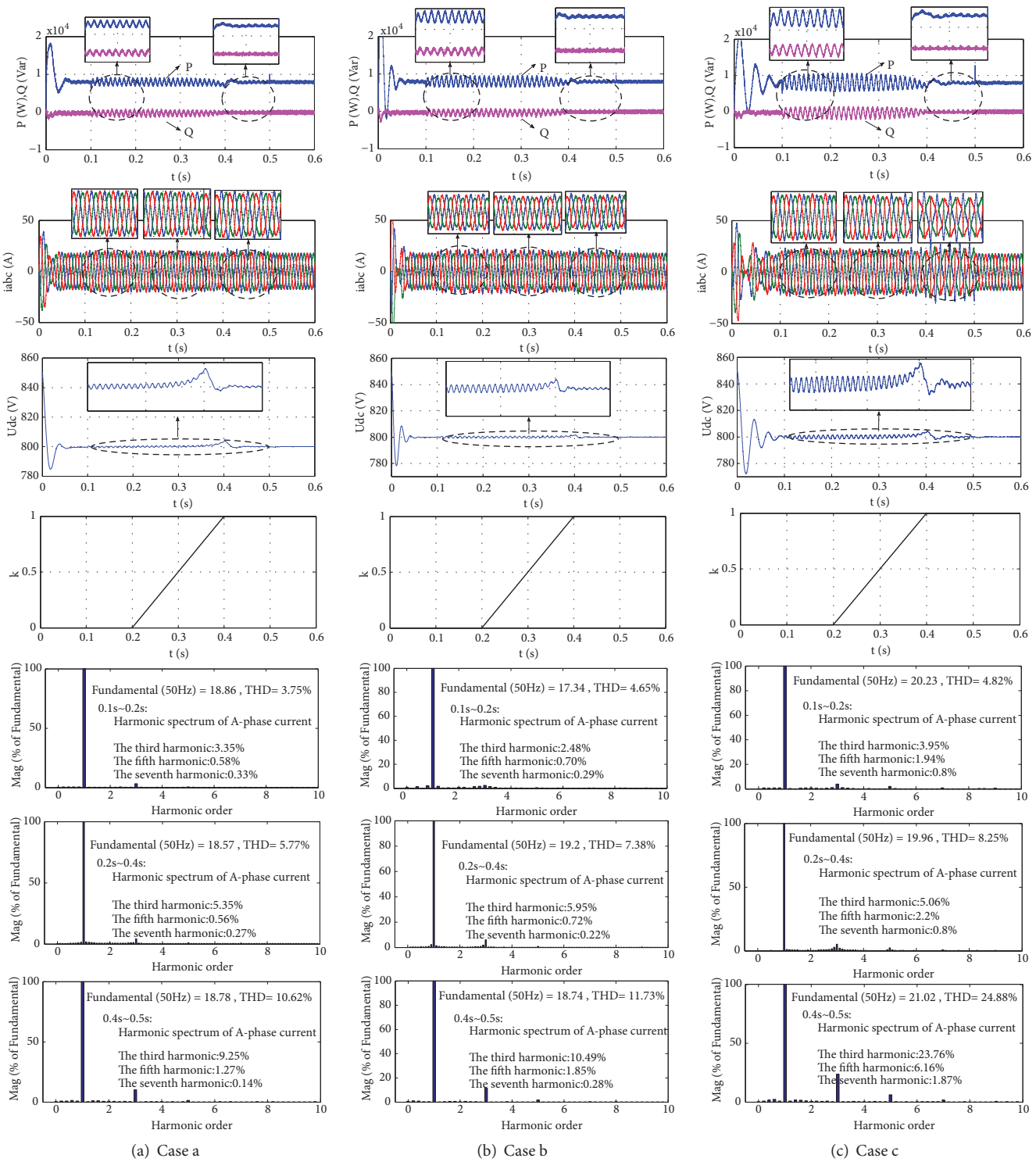

(a) Case a (b) Case b (c) Case c

Figure 14: Simulation results of using the control strategy proposed in Ref. [20] in different cases.

which is less than 5%. Therefore, the current balance control strategy can achieve good current quality, but the output power fluctuates significantly.

As can be seen from Figures 12 and 13, the instantaneous power control and current balance control cannot achieve the constant output power and good current quality simultaneously, which is consistent with the result of theoretical analysis.

Figure 14 shows the simulation results using the coordinate control strategy proposed in Ref. [20] in three different cases. The control scheme can judge and weigh the output power fluctuations and harmonic currents. However, notch

Table 2: Control effect comparison under different control strategies.

	Instantaneous power control	Current balance control	Control strategy is proposed in Ref. [20]	Proposed control
Constant power	Yes	No	Yes	Yes
Sinusoidal current	No	Yes	Yes	Yes
Balanced current	No	Yes	No	Yes

filter is needed in the control, the current references contain negative sequence components, and the balanced three-phase currents cannot be realized.

As can be seen from Figure 14, the weight coefficient $k = 0$ during the period of 0.1 s to 0.2 s, the harmonics of inverter currents are small, but the active and reactive powers fluctuate greatly. During the period of 0.4 s to 0.5 s, $k = 1$, the active and reactive powers are constant, but the harmonics of inverter currents are relatively large. As the value of k increases from 0 to 1, the three-phase inverter currents gradually change from sinusoidal curve to distorted curve, and the fluctuations on output power are gradually reduced, which realize the coordinate control of power and current. However, the current curves show that the balanced three-phase currents cannot be achieved. The simulation results are consistent with the theoretical analysis results.

Figure 15 shows the simulation results using the control strategy proposed in this paper. Theoretical analysis shows that, when k = 0, the reference of harmonic currents is zero, which is equivalent to the current balance control. From Figure 15, it can be observed that the output power fluctuates seriously during the period of 0.1 s to 0.2 s. However, the three-phase inverter currents are balanced and sinusoidal. Based on the analysis of phase A harmonic current spectrum, it can be seen that the THD is very small in the three cases (THD = 1.59%, THD = 2.37%, and THD = 3.35%, respectively) and there are little low-order harmonics, which are consistent with the theoretical analysis. Similarly, during the period of 0.4 s to 0.5 s, k = 1, while the nature of it, which is equivalent to instantaneous power control. The output active and reactive powers are constant, but the three-phase inverter currents are unbalanced and distorted. In the period of 0.2 s~0.4 s, the value of k increases from 0 to 1, and from the simulation results in this stage, it can be seen that, as k increases, the fluctuations on output power are decreased gradually, and the degrees of current unbalance and current distortion are increased. The simulation results verify the theoretical analysis. According to the above analysis, the coordinate control of output power and current can be realized by setting k in different applications, and the selection of the coefficient k in equation (18) should consider the THD of current and the fluctuations on output power based on the practical applications.

In order to verify the dynamic response ability of active and reactive powers with step change, the results of power and three-phase inverter currents in different cases are shown in Figure 16. In this verification, the active power reference is stepped from 8 kW to 15 kW at 0.4 s, while the reactive power reference is stepped from 0 kW to 5 kW for the construction of a friendly power grid. It can be seen that the output active power and reactive power have a step change at 0.4 s. At this stage, the proposed control can also be applied well. As k changes from 0 to 1, the fluctuations on output power decrease gradually, and the distortion degree of inverter currents increases gradually. After 0.5 s, the grid faults are eliminated, the active power and reactive power are almost constant, and inverter currents are sinusoidal. Therefore, the proposed control has no effect on the operation of the ideal grid, which shows that the proposed control is applicable to both ideal and unbalanced grid conditions. From Figure 16(c), it can be seen that, as the voltage drops dramatically, the peak value of the output currents is increased to maintain the output power. However, in practical applications, current limiting measures should be taken to prevent the harm of overcurrent, which has been studied in [22, 23]. This paper is not extended.

By analyzing the above results, the control effect comparison under different control strategies is listed in Table 2. Obviously, both instantaneous power control and current balance control can only control a single target, i.e., power or current. The control scheme proposed in Ref. [20] and the control proposed in this paper can realize the coordinate control of power and current.

In order to further analyze the control performance under these two coordinate control strategies, the performance comparison is shown in Table 3. Obviously, if the proposed control strategy is adopted, the settling time will be unchanged or increased in cases a and b, but other performance indicators have been proven to be more superior.

6. Conclusion

In this paper, coordinate control of power/current for grid-connected inverter is analyzed and studied under unbalanced grid voltage. The conclusions are as follows.

(1) Instantaneous power control and current balance control cannot meet constant power and balanced current simultaneously. Therefore, it is necessary to study the coordinate control of power/current.

(2) Based on the analysis of instantaneous power control and current balance control, the references of fundamental current under instantaneous power control are equal to the current reference values under current balance control, while the contents of harmonic currents under instantaneous power control determine the harmonic contents of inverter currents. Therefore, the coordinate control of power/current can be achieved by adjusting the harmonic contents under instantaneous power control.

Table 3: Control performance comparison of the coordinate control under different cases.

		Case a		Case b		Case c	
		Control in Ref. [20]	Proposed control	Control in Ref. [20]	Proposed control	Control in Ref. [20]	Proposed control
Current THD of phase-A (%)	0.1 s~0.2 s	3.75	1.59	4.65	2.37	4.82	3.35
	0.2 s~0.4 s	5.77	5.75	7.38	6.24	8.25	7.46
	0.4 s~0.5 s	10.62	7.00	11.73	8.26	24.88	10.15
DC-link voltage ripple (%)		0.47	0.21	0.21	0.18	0.51	0.27
Settling time (s)		0.10	0.10	0.09	0.10	0.12	0.11
Overshoot of DC-link voltage (%)		1.91	0.54	2.72	0.49	3.46	0.34
Amplitude of active power oscillations (% of P)		28.10	21.48	28.91	25.71	40.91	35.46
Amplitude of reactive power oscillations (% of P)		23.18	20.08	22.89	16.99	39.73	30.77

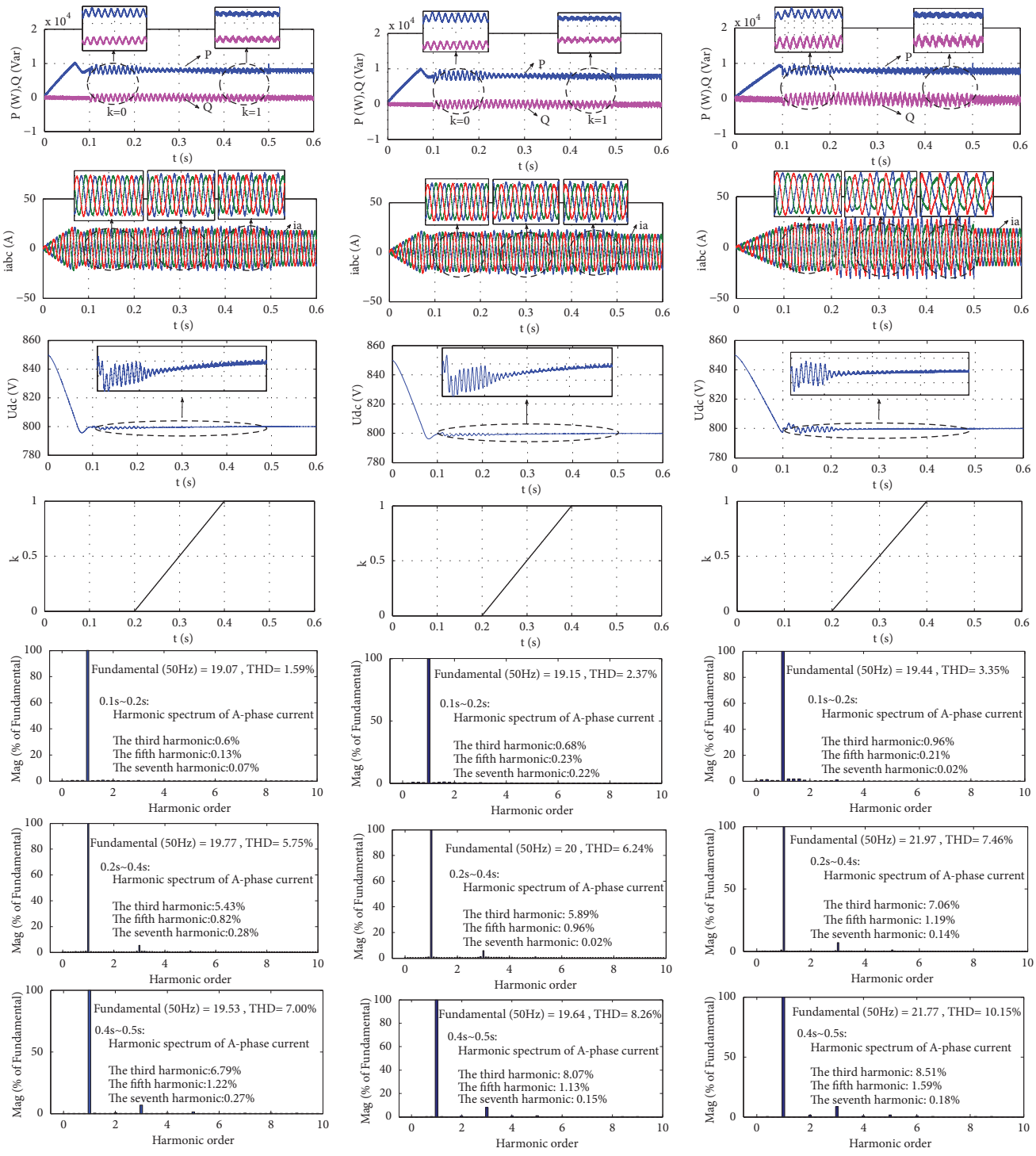

(a) Case a (b) Case b (c) Case c

Figure 15: Simulation results of proposed control strategy in different cases.

(3) The fundamental and harmonic currents can be controlled by PCI controller and PMCI controller, respectively. It is easy to realize in $\alpha\beta$ stationary reference frame without the complicated reference frame transformation and positive/negative sequence extraction calculation.

(4) The proposed control scheme does not need to detect the contents of low-order harmonics, nor does it need to use the notch filter. It is easy to realize the coordinate control of power fluctuation suppression and current balance by setting k in different conditions. The selection about the optimal

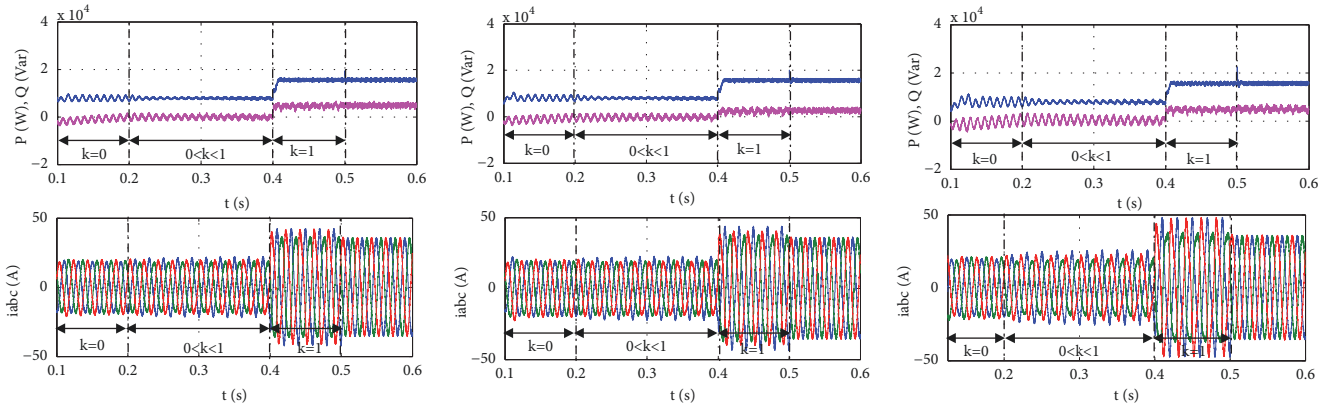

(a) Case a (b) Case b (c) Case c

Figure 16: Dynamic response ability of active power and reactive power with step change.

value of coefficient k is the future research direction and focus.

Data Availability

(1) The three-phase voltage data used to support the findings of this study are included within the article. (2) The circuit parameters (grid-side inductance, resistance, and dc-link voltage) data used to support the findings of this study are included within the article. (3) The controller parameters data used to support the findings of this study are included within the article.

Conflicts of Interest

The authors declare that there are no conflicts of interest regarding the publication of this paper.

Acknowledgments

The research was supported in part by the China Key R&D projects in Shaanxi (Grant no. 2017GY-061).

References

[1] Z. Li, Y. Li, P. Wang, H. Zhu, C. Liu, and W. Xu, "Control of three-phase boost-type PWM rectifier in stationary frame under unbalanced input voltage," *IEEE Transactions on Power Electronics*, vol. 25, no. 10, pp. 2521–2530, 2010.

[2] G. C. Konstantopoulos and A. T. Alexandridis, "Full-scale modeling, control and analysis of grid-connected wind turbine induction generators with back-to-back AC/DC/AC converters," *IEEE Transactions on Power Electronics*, vol. 2, no. 4, pp. 739–748, 2014.

[3] W. Jiang, W. Ma, J. Wang et al., "Deadbeat control based on current predictive correction for grid-connected converter under unbalanced grid voltage," *IEEE Transactions on Industrial Electronics*, vol. 64, no. 7, pp. 5479–5491, 2017.

[4] J. Hu and Y. He, "Modeling and control of grid-connected voltage-sourced converters under generalized unbalanced operation conditions," *IEEE Transactions on Energy Conversion*, vol. 23, no. 3, pp. 903–913, 2008.

[5] M. Castilla, J. Miret, J. L. Sosa, J. Matas, and L. G. de Vicuña, "Grid-fault control scheme for three-phase photovoltaic inverters with adjustable power quality characteristics," *IEEE Transactions on Power Electronics*, vol. 25, no. 12, pp. 2930–2940, 2010.

[6] J. Miret, M. Castilla, A. Camacho, L. G. De Vicuña, and J. Matas, "Control scheme for photovoltaic three-phase inverters to minimize peak currents during unbalanced grid-voltage sags," *IEEE Transactions on Power Electronics*, vol. 27, no. 10, pp. 4262–4271, 2012.

[7] X. Guo, W. Liu, and Z. Lu, "Flexible power regulation and current-limited control of grid-connected inverter under unbalanced grid voltage faults," *IEEE Transactions on Industrial Electronics*, vol. 34, no. 5, pp. 7425–7432, 2017.

[8] M. Castilla, J. Miret, A. Camacho, L. G. de Vicuna, and J. Matas, "Modeling and design of voltage support control schemes for three-phase inverters operating under unbalanced grid conditions," *IEEE Transactions on Power Electronics*, vol. 29, no. 11, pp. 6139–6150, 2014.

[9] K.-H. Kim, Y.-C. Jeung, D.-C. Lee, and H.-G. Kim, "LVRT scheme of PMSG wind power systems based on feedback linearization," *IEEE Transactions on Power Electronics*, vol. 27, no. 5, pp. 2376–2384, 2012.

[10] Y. S. Suh and T. A. Lipo, "Control scheme in hybrid synchronous synchronous stationary frame for PWM AC-DC converter under generalized unbalanced operating conditions," *IEEE Transactions on Industry Applications*, vol. 42, no. 3, pp. 825–835, 2006.

[11] H. S. Song and K. Nam, "Dual current control scheme for PWM converter under unbalanced input voltage conditions," *IEEE Transactions on Industrial Electronics*, vol. 46, no. 5, pp. 953–959, 1999.

[12] D. Wang, C. Liu, and G. Li, "Control scheme for photovoltaic three-phase inverters to minimize peak currents during unbalanced grid-voltage sags," *IEEE Transactions on Power Electronics*, vol. 27, no. 10, pp. 4262–4271, 2012.

[13] R. Teodorescu, M. Liserre, and P. Rodrguez, *Grid Converters for Photovoltaic and Wind Power Systems*, John Wiley and Sons, Ltd., Chichester, UK, 2011.

[14] P. Rodriguez, A. V. Timbus, R. Teodorescu, M. Liserre, and F. Blaabjerg, "Flexible active power control of distributed power

generation systems during grid faults," *IEEE Transactions on Industrial Electronics*, vol. 54, no. 5, pp. 2583–2592, 2007.

[15] C. T. Lee, C. W. Hsu, and P. T. Cheng, "A low-voltage ride-through technique for grid-connected converters of distributed energy resources," *IEEE Transactions on Industry Applications*, vol. 47, no. 4, pp. 1821–1832, 2011.

[16] W. Tao, Z. Gu, L. Wang et al., "Research on control strategy of grid-connected inverter under unbalanced voltage conditions," in *Proceedings of the Power Electronics and Motion Control Conference*, pp. 915–919, 2016.

[17] X. Li, Y. Tang, X. Wu et al., "Simplified multi-objective co-control to improve performance of three-phase grid-connected inverters under unbalanced grid conditions," *Energy, Power and Transportation Electrification*, pp. 1–6, 2017.

[18] A. Camacho, M. Castilla, and J. Miret, "Flexible voltage support control for three-phase distributed generation inverters under grid fault," *IEEE Transactions on Industrial Electronics*, vol. 60, no. 4, pp. 1429–1441, 2013.

[19] E. Afshari, G. R. Moradi, R. Rahimi et al., "Control strategy for three-phase grid-connected PV inverters enabling current limitation under unbalanced faults," *IEEE Transactions on Industrial Electronics*, vol. 64, no. 11, pp. 8908–8918, 2017.

[20] X. Guo, W. Liu, X. Zhang, X. Sun, Z. Lu, and J. M. Guerrero, "Flexible control strategy for grid-connected inverter under unbalanced grid faults without PLL," *IEEE Transactions on Power Electronics*, vol. 30, no. 4, pp. 1773–1778, 2015.

[21] X. Q. Guo and W. Y. Wu, "Improved current regulation of three-phase grid-connected voltage-source inverters for distributed generation systems," *IET Renewable Power Generation*, vol. 4, no. 2, pp. 101–115, 2010.

[22] M. M. Shabestary and A.-R. I. Mohamed, "An analytical method to obtain the maximum allowable grid support by using grid-connected converters," *IEEE Transactions on Sustainable Energy*, vol. 7, no. 4, pp. 1558–1571, 2016.

[23] M. Nasiri and R. Mohammadi, "Peak current limitation for grid side inverter by limited active power in PMSG-based wind turbines during different grid faults," *IEEE Transactions on Sustainable Energy*, vol. 8, no. 1, pp. 3–12, 2017.